AD-A115 643 DAVID W TAYLOR NAVAL SHIP RESEARCH AND DEVELOPMENT CE--ETC F/G 20/4
A LOCALIZED FINITE-ELEMENT METHOD FOR THREE DIMENSIONAL SHIP MO--ETC(U)
MAY 82 K J BAI
UNCLASSIFIED DTNSRDC-82/042 NL

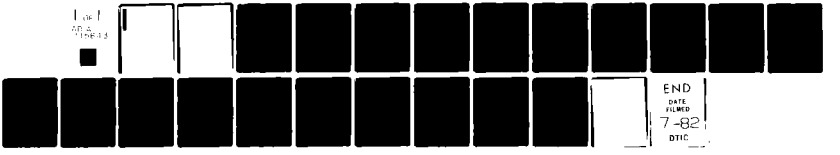

END
DATE FILMED
7-82
DTIC

UNCLASSIFIED

SECURITY CLASSIFICATION OF THIS PAGE *(When Data Entered)*

| REPORT DOCUMENTATION PAGE | | READ INSTRUCTIONS BEFORE COMPLETING FORM |
|---|---|---|
| 1. REPORT NUMBER<br>DTNSRDC-82/042 | 2. GOVT ACCESSION NO.<br>AD-A115643 | 3. RECIPIENT'S CATALOG NUMBER |
| 4. TITLE *(and Subtitle)*<br>A LOCALIZED FINITE-ELEMENT METHOD FOR THREE DIMENSIONAL SHIP MOTION PROBLEMS | | 5. TYPE OF REPORT & PERIOD COVERED<br>Formal<br>6. PERFORMING ORG. REPORT NUMBER |
| 7. AUTHOR(s)<br>Kwang June Bai | | 8. CONTRACT OR GRANT NUMBER(s) |
| 9. PERFORMING ORGANIZATION NAME AND ADDRESS<br>David W. Taylor Naval Ship Research and Development Center<br>Bethesda, Maryland 20084 | | 10. PROGRAM ELEMENT, PROJECT, TASK AREA & WORK UNIT NUMBERS<br>Task Area RR0140302<br>Work Unit 1542-018 |
| 11. CONTROLLING OFFICE NAME AND ADDRESS<br>Office of Naval Research (ONR-432)<br>Arlington, Virginia 22217 | | 12. REPORT DATE<br>May 1982<br>13. NUMBER OF PAGES<br>20 |
| 14. MONITORING AGENCY NAME & ADDRESS*(if different from Controlling Office)* | | 15. SECURITY CLASS. *(of this report)*<br>UNCLASSIFIED<br>15a. DECLASSIFICATION/DOWNGRADING SCHEDULE |

16. DISTRIBUTION STATEMENT *(of this Report)*

APPROVED FOR PUBLIC RELEASE: DISTRIBUTION UNLIMITED

17. DISTRIBUTION STATEMENT *(of the abstract entered in Block 20, if different from Report)*

18. SUPPLEMENTARY NOTES

19. KEY WORDS *(Continue on reverse side if necessary and identify by block number)*

Finite-Element Method
Ship Motion
Added Masses and Damping Coefficients
Restricted Water
Natural Frequency
Eigenvalues

20. ABSTRACT *(Continue on reverse side if necessary and identify by block number)*

An application of the localized finite-element method to a three-dimensional time-harmonic free surface flow in a canal is presented. Boundary conditions on both the free surface and the body are linearized and imposed on their equilibrium positions. By utilizing known set of eigenfunctions, the computation domain is reduced to a very small local domain where an eight-node linear three-dimensional element is used.

(Continued on reverse side)

DD FORM 1 JAN 73 1473 EDITION OF 1 NOV 65 IS OBSOLETE
S/N 0102-LF-014-6601

UNCLASSIFIED

SECURITY CLASSIFICATION OF THIS PAGE *(When Data Entered)*

(Block 20 continued)

Proper matching is also imposed between two sets of trial functions on the truncated boundary. To be solved are the problems concerning: (1) six degree-of-freedom radiation and diffraction in three dimensions, (2) two dimensional motion corresponding to the local flow at midship cross-sectional plane, and (3) related eigenvalues. Specifically, two sets of results for two ship locations in a canal are presented. In both cases, the eigenvalues of the local cross-sectional plane are shown to play a significant role in the three-dimensional results. A remarkable similarity between exciting forces and moment and the damping coefficients corresponding to the modes of their motions are also observed in the results. The accuracy of the three-dimensional results presented here is also discussed by comparing two sets of eigenvalues computed by using two different sizes of finite elements.

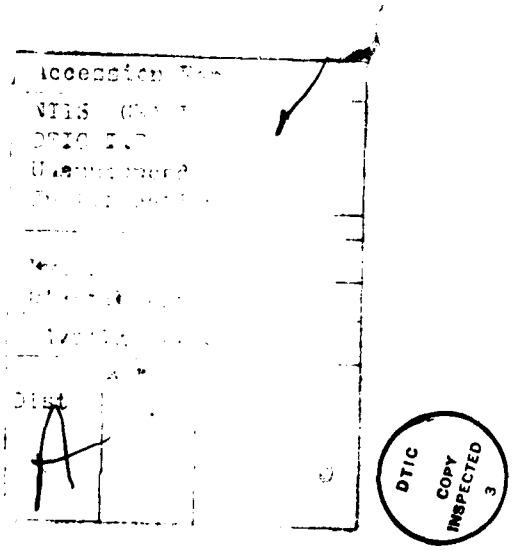

TABLE OF CONTENTS



LIST OF FIGURES

Page

# A LOCALIZED FINITE-ELEMENT METHOD FOR THREE DIMENSIONAL SHIP MOTION PROBLEMS*

Kwang June Bai
David W. Taylor Naval Ship Research and Development Center
Bethesda, Maryland 20084

## Abstract

An application of the localized finite-element method to a three-dimensional time-harmonic free surface flow in a canal is presented. Boundary conditions on both the free surface and the body are linearized and imposed on their equilibrium positions. By utilizing known set of eigenfunctions, the computation domain is reduced to a very small local domain where an eight-node linear three-dimensional element is used. Proper matching is also imposed between two sets of trial functions on the truncated boundary. To be solved are the problems concerning: (1) six degree-of-freedom radiation and diffraction in three dimensions, (2) two dimensional motion corresponding to the local flow at the midship cross-sectional plane, and (3) related eigenvalues. Specifically, two sets of results for two ship locations in a canal are presented. In both cases, the eigenvalues of the local cross-sectional plane are shown to play a significant role in the three-dimensional results. A remarkable similarity between exciting forces and moment and the damping coefficients corresponding to the modes of their motions are also observed in the results. The accuracy of the three-dimensional results presented here is also discussed by comparing two sets of eigenvalues computed by using two different sizes of finite elements.

## I. Introduction

Steady-state time-harmonic motions of an inviscid, incompressible fluid with free surface in the presence of a body or bodies in it are described by a boundary-value problem governed by the Laplace equation with appropriate boundary conditions. In the past, problems of this type were generally solved by distributing sources (and/or dipoles) on the body boundary and using Green's theorem to obtain an integral equation for the strength of these boundary singularities; or, alternatively, by using sources and higher-order multipole expansions at an interior point within the body, the strengths of these singularities being determined so as to satisfy the body boundary condition. In all cases it is conventional to utilize the singularities which are solutions of the boundary-value problem stated above, except for the body boundary condition which is invoked separately to determine the singularity distribution.

For two- and three-dimensional motions in a fluid of infinite depth, or of finite but constant depth, the required singularities are well known, although of rather complicated analytical form, so that the approach described in the foregoing corresponds to solving a Fredholm integral equation over the body surface, with a rather complicated kernel function. An extensive list of literature on this subject can be found in Wehausen[1].

In this paper a numerically oriented as well as more versatile method is introduced as an alternative approach to the solution of the problem. This alternative approach is based on a variational principle which is utilized to determine the velocity potential throughout the fluid domain. The present work is a direct extension of the earlier work by Bai and Yeung[2] for a general three-dimensional body geometry in a canal. In this procedure, the known solution space in certain subdomains is made use of in order to reduce the 'computation box' to a size as small as possible. We call this drastically-reduced computation box the localized finite-element domain. The phrase "localized finite-element method" is used to denote the finite element method applied only in this localized subdomain. In this particular problem, i.e., in a free-surface flow in a canal, the solution space is represented by the complete set of eigenfunctions in the subdomain. It is essential to make the domain of computation as small as possible because the practical success or failure of a numerical method, in general, mainly depends upon the size of the computation box. In the present procedure, the reduction of the original infinite fluid domain to a small localized subdomain is achieved by replacing the conventional radiation condition by the matching condition. This requires that the velocity potential and its normal derivative (i.e., normal velocity) represented by two sets of different trial functions, defined in the adjacent subdomains, be continuous along the fictitious interface juncture boundary surface. Then we approximate the potential in the localized finite-element domain by piecewise polynomial trial functions defined in each finite element. Thus, in effect, an integral equation over a body surface with a complicated kernel is replaced by a system of equations over a much larger fluid domain, but with a much simpler kernel.

Previous studies of the finite element method applied to time-harmonic ship motion problems have been made by Bai[3-6], Berkhoff[7], Smith[8], Chen and Mei[9], Seto and Yamamoto[10], Yue et al[11], Euvrard et al[12], and Chowdbury[13].

Additional numerical results of the related two-dimensional boundary-value and eigenvalue problems at the midship cross-sectional plane are also presented. Two different sizes of the finite elements in the midship cross-sectional plane are used in these additional computations. These results are used as reference in discussing the accuracy of the present three-dimensional results.

*This work was supported by the Numerical Naval Hydrodynamics Program at the David W. Taylor Naval Ship R&D Center. This Program is jointly supported by NSRDC and the Office of Naval Research. Part of the present work was done while the author was a visiting professor at the Ecole Nationale Superieure de Techniques Avancees (ENSTA) in 1980, and partially supported by the Ministry of Defense, France.

## II. Mathematical Formulation

Considered here is steady-state time-harmonic free-surface flow in the presence of a body floating or submerged in a canal with a rectangular uniform cross-section. However, a local variation of the bottom and side-wall geometry is present and a uniform rectangular cross-section of each side (not necessarily the same on both sides), can be similarly treated by the present method. The coordinate system is right-handed and rectangular. The y-axis is directed opposite to the force of gravity, and the xz-plane coincides with the undisturbed free surface. The bottom of the canal is in the $y = -H$ plane and the side walls are in the $z = \pm W/2$ planes. We neglect surface tension, and assume that the fluid is inviscid and incompressible and that the motion is irrotational. Furthermore, we assure that the motion of the body and, consequently, the generated wave, to be small in some sense, so that the boundary condition on the body and on the free surface can be linearized and satisfied at the mean equilibrium positions instead of at their instantaneous positions.

Let $\Phi(x, y, z, t)$ be the velocity potential describing the flow field. The continuity equation requires $\Phi$ to satisfy Laplace's equation. Let $\sigma$ be the angular frequency of the time-harmonic solution. Then, introducing the usual time and spatial decomposition we have

$$\Phi(x, y, z, t) = Re\left[\phi^{(m)}(x, y, z)\, a^{(m)}(t)\right] \tag{1}$$

$$m = 1, \ldots, 7$$

where
$$\phi^{(m)} = \phi_1^{(m)} + i\phi_2^{(m)} \tag{2}$$

is the complex-valued spatial potential, and $a^{(m)}(t)$ is the complex time-harmonic motion amplitude of the body corresponding to the m-th mode, i.e.,

$$\begin{aligned} a_m(t) &= Re\left[a^{(m)}(t)\right] \\ &= Re\left[\left(a_1^{(m)} + ia_2^{(m)}\right)e^{-i\sigma t}\right] \end{aligned} \tag{3}$$

where $a_m(t)$ is the body motion amplitude. For $m = 7$, the diffraction problem corresponding to an incoming wave system of unit amplitude, one simply sets $a_1^{(7)} = 0$ and $a_2^{(7)} = 1/\sigma$ in Equation (3). The potential function $\phi(x, y, z)$ must satisfy

$$\left(\frac{\partial^2}{\partial x^2} + \frac{\partial^2}{\partial y^2} + \frac{\partial^2}{\partial z^2}\right)\phi(x, y, z) = 0 \tag{4}$$

in the fluid,

$$\phi_y - \nu\phi\big|_{S_F} = 0 \tag{5a}$$

$$\phi_n\big|_{S_O} = V_n = f(s) \tag{5b}$$

$$\phi_n\big|_{S_B} = 0 \tag{5c}$$

$$\phi_n\big|_{S_W} = 0 \tag{5d}$$

where $\nu = \sigma^2/g$
$g$ — acceleration due to gravity
$S_F$ — undisturbed free surface, $y = 0$, outside of the body
$S_B$ — bottom surface
$S_W$ — side walls
So — body surface below the mean free surface.

The normal velocity $f(s)$ depends upon the mode index m. For $m = 1, 2, \ldots, 6$, corresponding to the sway, heave, surge, roll, pitch, and yaw modes of motion, respectively, $f(s)$ is given by

$$f^{(i)}(s) = n_i \tag{6}$$

with

$$(n_1, n_2, n_3) = (n_x, n_y, n_z)$$

$$(n_4, n_5, n_6) = (\vec{r} - \vec{r}_c) \times \vec{n}$$

where $\vec{n}$ is the unit normal vector into the body with components $(n_x, n_y, n_z)$, $\vec{r}_c$ is the vector from the origin to the center of rotation, and

$$\vec{r} = (x, y, z).$$

For $m = 7$,
$$f(s) = \frac{-\partial\phi_I}{\partial n} \tag{7}$$

where $\phi_I$ is the spatial potential associated with the incident wave system. The incident wave potential of unit amplitude incoming from $x = -\infty$ is given by

$$\phi_I(x, y, z) = -\frac{g}{\sigma}\frac{\cosh m_o(y + H)}{\cosh m_o H}\, e^{im_o x} \tag{8}$$

where $m_o$ is wave number. Finally, to make the solution of this problem unique, we impose the radiation condition requiring that the generated waves must be outgoing.

## III. Localized Finite Element Method

The fluid domain defined in the foregoing formulation is unbounded along the x-axis. For numerical computations, it is highly desirable that the computation box be made as small as possible. The goal of reducing the original infinite fluid domain to a manageable finite domain is achieved by making use of the known solution space in the truncated infinite subdomains which will be defined later. As a result, the computation domain is reduced to a very local subdomain, called a localized finite element domain, which may barely include any source of disturbance in the fluid. The present numerical method is called a localized finite element method because the finite element numerical computations are made only for a local domain. Throughout this section, the subscript m in the potential, defined in the Mathematical Formulation section is omitted with the understanding that $\phi$ will always depend upon m.

Let us draw two imaginary vertical planes $J_1$ and $J_2$ which separate the original fluid domain D into the three subdomains: $D_o$, $D_1$, $D_2$ as shown in Figure 1. We assure that $D_o$ includes the ship (and/or any other sources of disturbance). The boundary surfaces $\partial D_o$, $\partial D_1$, and $\partial D_2$ are denoted, respectively, as

$$\begin{aligned} \partial D_o &= S_{Fo} + S_{Wo} + S_{Bo} + J_1 + J_2 + S_o \\ \partial D_i &= S_{Fi} + S_{Wi} + S_{Bi} + J_i + S_{Ri} \qquad i = 1,2 \end{aligned} \tag{9}$$

where $S_{Fi}$, $S_{Bi}$, and $S_{Wi}$, denote, respectively, the free surface, the bottom, and the canal side walls, in the subdomains $D_i$ (for $i = 0, 1, 2$) and where $S_{Ri}$ (for $i = 1, 2$) are the boundaries at infinity. The ship hull surface is denoted by $S_o$.

Let $\phi_o$, $\phi_1$, and $\phi_2$ denote the velocity potentials defined in the subdomains $D_o$, $D_1$, and $D_2$, respectively. Then we have, from Equations (4) and (5),

$$\begin{aligned} \nabla^2\phi_o &= 0 && \text{in } D_o \\ \phi_{on} - \nu\phi_o &= 0 && \text{on } S_{Fo} \\ \phi_{on} &= f(s) && \text{on } S_o \\ \phi_{on} &= 0 && \text{on } S_{Bo} \cup S_{Wo} \end{aligned} \tag{10}$$

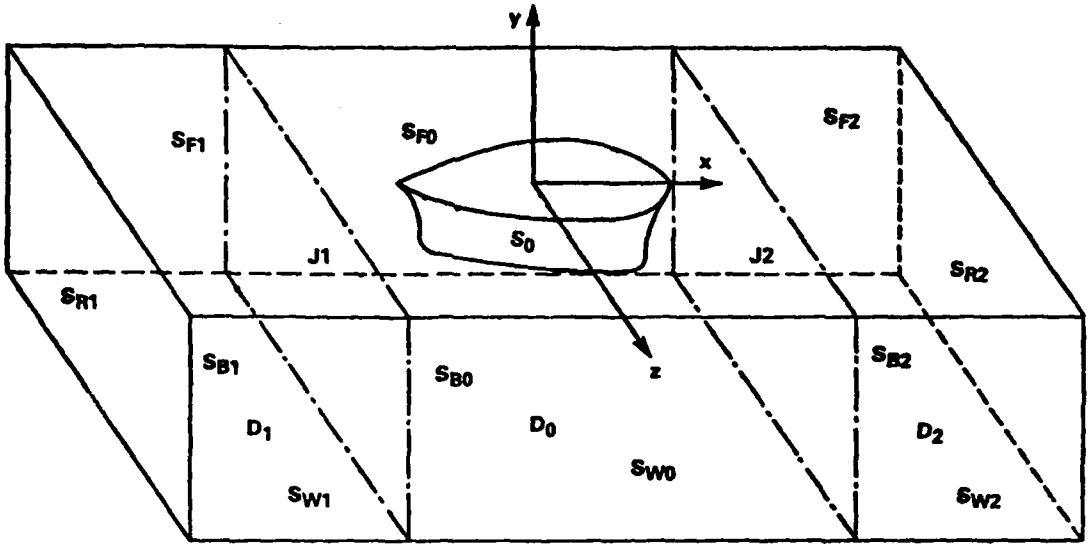


Figure 1 – Boundary Configurations of the Three Subdivided Fluid Domains

and, for $\phi_i$, i = 1, 2,

$$\begin{aligned} \nabla^2 \phi_i &= 0 && \text{in } D_i \\ \phi_{in} - \nu\phi_i &= 0 && \text{on } S_{Fi} \\ \phi_{in} &= 0 && \text{on } S_{Bi} \cup S_{Wi} \end{aligned} \tag{11}$$

It is understood in Equation (11) that a proper radiation condition is imposed at infinities for $\phi_1$ and $\phi_2$. In addition, we require

$$\left.\begin{aligned} \phi_o &= \phi_i \\ \phi_{on} + \phi_{in} &= 0 \end{aligned}\right\} \quad \text{on } J_i,\ i = 1, 2 \tag{12}$$

where the normal vector is taken outwards from the fluid subdomain defined for each potential, e.g.,

$$\begin{aligned} \phi_{1n} &= \phi_{1x}, \quad \phi_{on} = -\phi_{ox} && \text{on } J_1 \\ \phi_{2n} &= -\phi_{2x}, \quad \phi_{on} = \phi_{ox} && \text{on } J_2 \end{aligned} \tag{13}$$

By the juncture conditions in Equations (12), the solutions of Equations (10) through (12) are unique and identical to the solution of the original formulation in the Mathematical Formulation section. (This can be shown by applying Green's theorem to the difference of the solution of the original equation, defined in the previous section, and the solutions $\phi_o$, $\phi_1$, and $\phi_2$, defined in the three subdomains).

Let us assume that the general solutions of Equation (11) with appropriate radiation conditions, are known, i.e., the complete set of eigenfunctions or Green's functions of the problems. Then the first step toward the construction of the appropriate functional for our variational equation equivalent to the coupled partial differential equations defined in (10) through (12) is the choice of trial function space for each function $\phi_o$, $\phi_1$, and $\phi_2$. If the bases of the trial functions for $\phi_1$ and $\phi_2$ are chosen from the solution space (the known general solutions), then we can obtain the following two functionals:

$$K_1\{\phi_o,\phi_1,\phi_2\} = \iiint_{D_o} \tfrac{1}{2}(\nabla\phi_o)^2 dv - \tfrac{\nu}{2}\iint_{S_{Fo}} \phi_o^2 ds - \iint_{S_o} f(s)\phi_o ds + \iint_{J_1} (\phi_o - \tfrac{1}{2}\phi_1)\phi_{in} ds + \iint_{J_2} (\phi_o - \tfrac{1}{2}\phi_2)\phi_{2n} ds \tag{14}$$

and

$$K_2\{\phi_o,\phi_1,\phi_2\} = \iiint_{D_o} \tfrac{1}{2}(\nabla\phi_o)^2 dv - \tfrac{\nu}{2}\iint_{S_{Fo}} \phi_o^2 ds - \iint_{S_o} f(s)\phi_o ds + \iint_{J_1} [(\phi_1 - \phi_o)\phi_{on} + \tfrac{1}{2}\phi_1\phi_{1n}] ds + \iint_{J_2} [(\phi_2 - \phi_o)\phi_{on} + \tfrac{1}{2}\phi_2\phi_{2n}] ds \tag{15}$$

Setting the first variation of either functional to be zero, i.e.,

$$\delta K_1\{\phi_o, \phi_1, \phi_2\} = 0 \tag{16a}$$

or

$$\delta K_2\{\phi_o, \phi_1, \phi_2\} = 0 \tag{16b}$$

is the same as solving Equations (10) through (12). It is easy to show this by taking the first variation and by using Green's theorem[2]. The integral expressions of the functionals involve only the subdomain $D_o$ which we call the "localized finite-element domain." If one takes the localized finite-element domain to be small, then the domain over which the integrals have to be computed will also be small. On the other hand, one has to take many terms (eigenfunc-

tions) to represent the trial solutions $\phi_1$ and $\phi_2$ in the computation of the approximate solutions, and vice versa.

It is interesting that the stationary value of both functions are

$$K_1\{\phi_o, \phi_1, \phi_2\} = -\frac{1}{2}\iint_{S_o} f(s)\,\phi_o\,ds \tag{17a}$$

$$K_2\{\phi_o, \phi_1, \phi_2\} = -\frac{1}{2}\iint_{S_o} f(s)\,\phi_o\,ds \tag{17b}$$

if $\phi_o$, $\phi_1$, and $\phi_2$ are the exact solutions. This stationary value is simply $(-1/2\varrho)$ times the added mass and $(-1/2\varrho\omega)$ times the damping coefficients.

Either functional, defined in (14) or (15), will give a variational equation mathematically equivalent to the original boundary-value problem at hand. The use of the functional given in (14) is slightly advantageous because the normal derivative of $\phi_o$ is not involved in the coupling integral terms. In the present computation, the functional given in Equation (14) is used. The equivalence of the differential equation to the variational problem is basic to the choice of the computational scheme. One significant difference between the functional method and the differential equation is the fact that the expressions for the associated functionals in (14) and (15) involve no second derivatives, owing to the integration by parts used to construct these functionals, i.e., Green's theorem is used here. It follows that the functionals will be well defined if only the first derivative of the function, rather than the second, is required to be bounded. Therefore, the class of admissible functions, in the problem to find the stationary point, is enlarged to a space bigger than that for the original differential equation. We now have the advantage, while searching for the stationary point of the functional, of being permitted to try functions outside the class of those originally admissible. In practice, this means that we can now try continuous functions whose first derivatives are only piecewise continuous. In other words, the first derivative can have finite discontinuities at the juncture boundary between adjacent elements. It is very easy to construct basis functions that satisfy the previous requirements.

In the localized finite element domain $D_o$, the basis for the trial function is chosen from a polynomial basis. Specifically, eight-node isoparametric, linear three-dimensional elements were used in the present numerical calculations. As mentioned earlier, the trial functions in $D_1$ and $D_2$ will be chosen from a subspace of the solution space which satisfies the Laplace equation with the free-surface condition, the side-wall condition, the bottom condition, and the radiation condition at infinity. The eigenfunctions or the Green functions of the above problem can represent the solution space. However, we will choose the eigen-function space in this paper for its simplicity.

The variational equation (16a) goes into operational form in the following way. Let $q_{ij}$ ($i = 0, 1, 2$, and $j = 1, 2, \ldots M_i$) be the basis for the trial functions in each subdomain $D_i$ ($i = 0, 1, 2$). Then the solution is assumed to be

$$\phi_i = \sum_{j=1}^{M_i} \varphi_{ij}\, q_{ij} \tag{18}$$

in $D_i$ ($i = 0, 1, 2$), where $\varphi_{ij}$ are coefficients to be determined. By substituting Equation (18) in the functional defined in Equation (14), the variational equation (16a) reduces to a set of linear algebraic equations. (In this procedure, only the coefficients are subject to variation.)

A complete set of eigenfunctions (the resonance frequencies are excluded) are given in Wehausen[14] as

$$\left\{ e^{\mp i K_{no} x}\, \frac{\cosh m_o (y + H)}{\cosh m_o H} \cos \frac{n\pi}{W}\left(z - \frac{W}{2}\right),\right.$$
$$\left. e^{\pm K_{np} x} \cos m_p (y + H) \cos \frac{n\pi}{W}\left(z - \frac{W}{2}\right)\right\} \tag{19}$$

where W is the width of the tank and the upper and lower signs are to be taken in the subdomains $D_1$ and $D_2$, respectively, and where

$$K_{no} = \left[m_o^2 - \left(\frac{n\pi}{W}\right)^2\right]^{\left(\frac{1}{2}\right)}$$
$$K_{np} = \left[m_p^2 + \left(\frac{n\pi}{W}\right)^2\right]^{\left(\frac{1}{2}\right)} \tag{20}$$

and $m_o$ and $m_p$ ($p = 1, 2, \ldots$) are the real roots of

$$m_o \tanh m_o H = \nu$$
$$m_p \tan m_p H = -\nu \tag{21}$$

The exponent of the first term in Equation (19) becomes real when $n\pi/W > m_o$, resulting in a local disturbance, and if $n = 0$, it becomes purely a two-dimensional case. The case when $m_o = n\pi/W$ ($n = 1, 2, \ldots$), i.e., the case of resonance, is left out in the present study. Here we considered only the case of $m_o \neq n\pi/W$.

## IV. Results and Discussions

After the potential $\phi^{(i)}$, defined in the Mathematical Formulation section, has been computed, the hydrodynamic coefficients can be computed by

$$\bar{\mu}_{ij} + \frac{i}{\sigma}\bar{\lambda}_{ij} = \varrho \iint_{S_o} \phi^{(i)} n_j\, ds \tag{22}$$

where $\bar{\mu}_{ij}$ are the added masses for i, j = 1, 2, 3, moments of added mass for i (or j) = 1, 2, 3 and j (or i) = 4, 5, 6, and moments of inertia of added mass for i, j = 4, 5, 6, and where $\bar{\lambda}_{ij}$ (i, j = 1, . . . , 6) are the damping coefficients. In presenting our results, the nondimensional hydrodynamic coefficients, $\mu_{ij}$ and $\lambda_{ij}$ are defined by using the ship displacement V and the ship length L as follows:

$$\mu_{ij} = \bar{\mu}_{ij}/\varrho V, \qquad \lambda_{ij} = \bar{\lambda}_{ij}/\varrho\omega V \qquad j = 1, 2, 3$$

$$\mu_{ij} = \bar{\mu}_{ij}/\varrho VL, \qquad \lambda_{ij} = \bar{\lambda}_{ij}/\varrho\omega VL \qquad \text{or} \qquad \begin{matrix} i = 1, 2, 3, j = 4, 5, 6 \\ i = 4, 5, 6, j = 1, 2, 3 \end{matrix} \tag{23}$$

$$\mu_{ij} = \bar{\mu}_{ij}/\varrho VL^2, \qquad \lambda_{ij} = \bar{\lambda}_{ij}/\varrho\omega VL^2 \qquad i, j = 4, 5, 6$$

where $V = L\,B\,T$ is the ship displacement volume. The results of wave excitation forces and moments are also similarly nondimensionalized by using the unit amplitude

of the incoming wave, Y = 1, and the ship length L as

$$\left.\begin{aligned} F_i &= \bar{F}_i/\rho g Y L^2 \\ M_i &= \bar{M}_i/\rho g Y L^3 \end{aligned}\right\} i = 1, 2, 3 \qquad (24)$$

where

$$\bar{F}_i = -i\omega\rho \iint_{S_o} (\phi^{(7)} + \phi_I)\, n_i\, ds$$

$$\bar{M}_i = -i\omega\rho \iint_{S_o} (\phi^{(7)} + \phi_I)\, n_{i+3}\, ds \qquad (25)$$

In the present computations, a rectangular barge which floats parallel to the tank walls, i.e., the angle between the center plane of the barge and the xy-plane is zero, is treated for its simplicity in data preparation. However, any arbitrary angle and ship geometry can be handled by the present computer program. The midship section plane is assumed to coincide with the yz-plane for the present test model. The cross-section of the canal at the origin, i.e., the yz-plane is given in Figure 2. We denote the distance between the ship center-plane and the xy-plane by s, as shown in Figure 2. The moment is computed with respect to the centroid of the ship's water-plane area, i.e., $\bar{r}_c = (0, 0, s)$ in Equation (6). In presenting our numerical results, the nondimensional wave number, $\nu B = \omega^2 B/g$ is plotted along the abscissa.

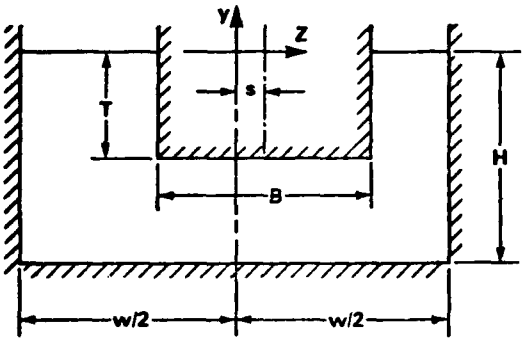


Figure 2 – Cross-Section at x=0

In the present computations, two locations of the body in a canal are computed; first, the ship is located at the center of the canal, i.e., s/B = 0, and second, the ship is at an off-center location in a canal. In both cases, the ship is parallel to the canal walls, as mentioned earlier. Specifically, the computations are made for W/B = H/T = W/H = B/T = 2 and L/T = 10 for both values of s/B = 0 and 0.125. Before we compute these two cases, we have done computations for a two-dimensional rectangular cylinder which is uniform between two walls, i.e., the cylinder lies normal to the xy-plane. These test results were compared with those computed by the results of our previous work in two-dimensional problems. The comparison was good.

Several sets of finite element subdivisions were initially tested in the present study. The total number of nodes tested are 180, 350, 507, 1404, and 1782 (the corresponding numbers of nodes on the ship boundary are, 44, 81, 81, 249, and 249, respectively). The indices n in the eigenfunction (Equation (19)) were taken between 6 and 10, and while the indices p were taken between 6 and 10 for n = 0, the values of p were reduced as n increased. The present computations were made for the range of non-dimensional wave numbers, $2\pi/m_o L = 0.52$ through 2.72. This range was selected partly due to the limitation of numerical accuracy without taking very small finite elements, while the first mode of canal resonance, i.e., when $m_o W/\pi = 1$ (see the text following Equation (21)), is included. This first mode of the canal resonance, $m_o W/\pi = 1$, corresponds to $\nu B = 1.44066$ in the present ship-canal geometry.

Considering the wave number range to be tested and the computation time, we decided to use the 507-node model throughout the present computations. In subdividing the localized finite-element domain into a number of finite elements, we used four equal elements along the depth and four equal elements across the width of the canal. Five equal elements were used along both sides of the x-axis and five more elements were used further along both sides of the x-axis. The ship replaces the middle ten elements along the x-axis and the middle two elements along the z-axis and the two elements along the depth from the free surface. When the ship is at an off-center location in a canal, we simply stretch the elements on one side and shrink those on the other side mainly for the ease of data preparation, especially for the case when the off-center distance is not too great. Any complicated situation can be accommodated by the present method but only through more tedius data preparation.

For all cases treated here, the computations were made for 23 values of $\nu B$ between 0.2 and 2.4 with a constant increment of 0.1 throughout the present computations. Then the 23 computed values of the hydrodynamic coefficients were plotted by a computer using a straight-line interpolation.

The computational results for the case when the ship is located at the center of a canal are presented in Figures 3 through 6. Figure 7 shows the hydrodynamic coefficients computed for the midship section, i.e., the yz-plane as a purely two dimensional problem with no wave radiation present. The result for a two-dimensional model provides the resonance mode which plays a significant role in the local flow field in three-dimensional problem.

In Figure 3, the computed values of added mass and moment of inertia of added mass are shown. The surge added-mass coefficient, $\mu_{11}$, shows an oscillatory behavior, being approximately zero at $\nu B = 0.9$ and reaching a local maximum at $\nu B = 1.4$. The heave added-mass coefficient $\mu_{22}$ is negative approximately between $\nu B = 0.20$ and 1.20. Both sway added-mass coefficients $\mu_{33}$ and roll moment of inertia of added mass $\mu_{44}$ change abruptly from positive peak values to negative peak values between $\nu B = 0.9$ and 1.0. A similar behavior is also observed in the yaw moment of inertia of added mass $\mu_{55}$ between $\nu B = 1.2$ and 1.3. The pitch moment of inertia of added mass $\mu_{66}$ is minimum around $\nu B = 1.3$.

In Figure 4, the six diagonal damping coefficients, $\lambda_{ii}$ (i = 1, 6), are shown for s/B = 0. The value of $\lambda_{11}$ decreases with increasing value of $\nu B$, and is approximately zero at $\nu B = 1.2$ and reaches a local maximum at 1.8. The values of $\lambda_{22}$ decrease monotonically and also rapidly to zero at $\nu B = 1$. The values of $\lambda_{33}$ and $\lambda_{44}$ are zero between $\nu B = 0.2$ and 1.4, then sharply increase to local maxima at 2.0, and finally decrease. The value of $\lambda_{55}$ shows a behavior similar to $\lambda_{33}$ and $\lambda_{44}$, but becomes zero again at $\nu B = 2.0$ and increases again. The pitch damping coefficient $\lambda_{66}$ decreases rather rapidly to zero between $\nu B = 1.0$ and 1.8. It is of interest to note that the values of $\lambda_{33}$, $\lambda_{44}$, and $\lambda_{55}$ are zero for $\nu B \leq 1.4$. This is because the flow fields for the sway, roll, and yaw motions are purely due to local disturbances when $\nu B < \pi/2 \tanh \pi/2 = 1.4406\cdots$ (this value corresponds to the first mode over the canal resonance). (Note that the motions are asymmetric with respect to the xy-plane while the only admissible far-field wave solution is pure two-dimensional).

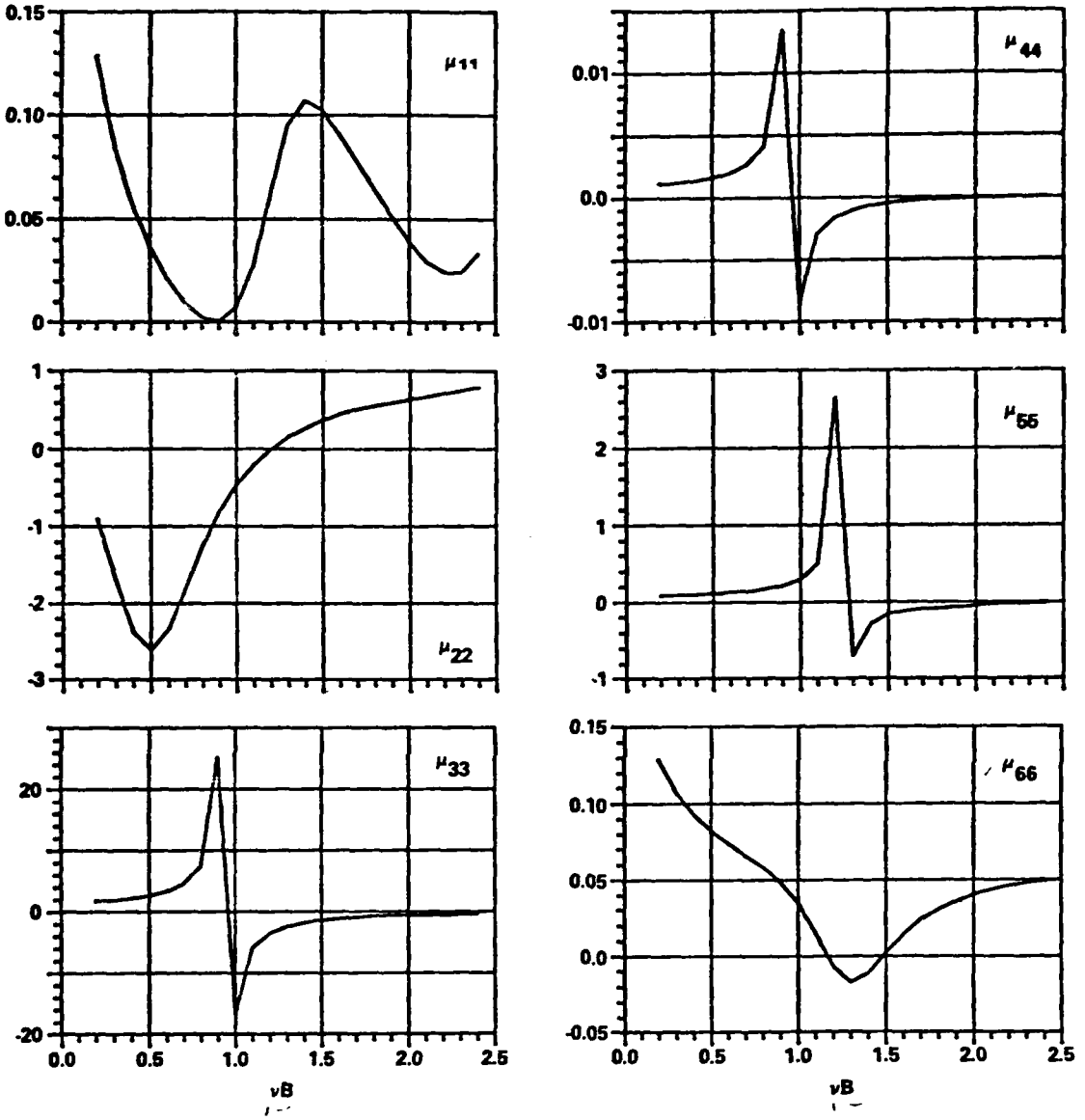


**Figure 3 — Added Masses, and Moments of Inertia of Added Mass, $\mu_{ij}$ versus νB, for s/B = 0**

Due to the symmetry of the body and the canal geometry with respect to the xy-plane and the yz-plane, there are only four nonzero coupling hydrodynamic coefficients. These are shown in Figure 5. The pitch moment of surge added mass $\mu_{16}$ reaches a maximum at $\nu B = 1.1$ and then decreases. The roll-sway coupling term $\mu_{34}$ changes abruptly from a negative peak to a positive peak between $\nu B = 0.9$ and 1.0. The surge-pitch coupling damping coefficient $\lambda_{16}$ is a maximum at $\nu B = 1.4$ and slowly decreases to a positive constant. The sway-roll coupling damping coefficient $\lambda_{34}$ is zero, as discussed earlier, between $\nu B = 0.2$ and 1.4, reaches a negative peak sharply, and then increases.

In Figure 6, the magnitudes of the wave excitation forces and moment are shown. The magnitude of the surge excitation force $|F_1|$ reaches a local minimum at $\nu B = 1.2$ and a local maximum at 1.6. The magnitude of the heave excitation force $|F_2|$ decreases monotonically from its value at $\nu B = 0.2$ to zero at 1.2 and then reaches a local maximum at 1.8. It is of interest to note that the zero value of the heave excitation force would be at $\nu B = 1.0683$, which gives an incident wavelength equal to the ship length, if the Froude-Krylov approximation is made; this value is not too far from the computed result of $\nu B = 1.2$. The magnitude of the pitch excitation moment decreases from a local maximum of zero at $\nu B = 1.8$ and slowly increases to the next local maximum. The rest of the other excitation forces and moments, not shown here, are all zero, due to symmetry in the problem.

It should be noted in comparing the damping coefficients $\lambda_{11}$, $\lambda_{22}$, and $\lambda_{66}$ in Figure 4, the excitation forces $|F_1|$ and $|F_2|$, and the moment $|M_3|$, in Figure 6, respectively. There exists a close similarity in the behavior of the

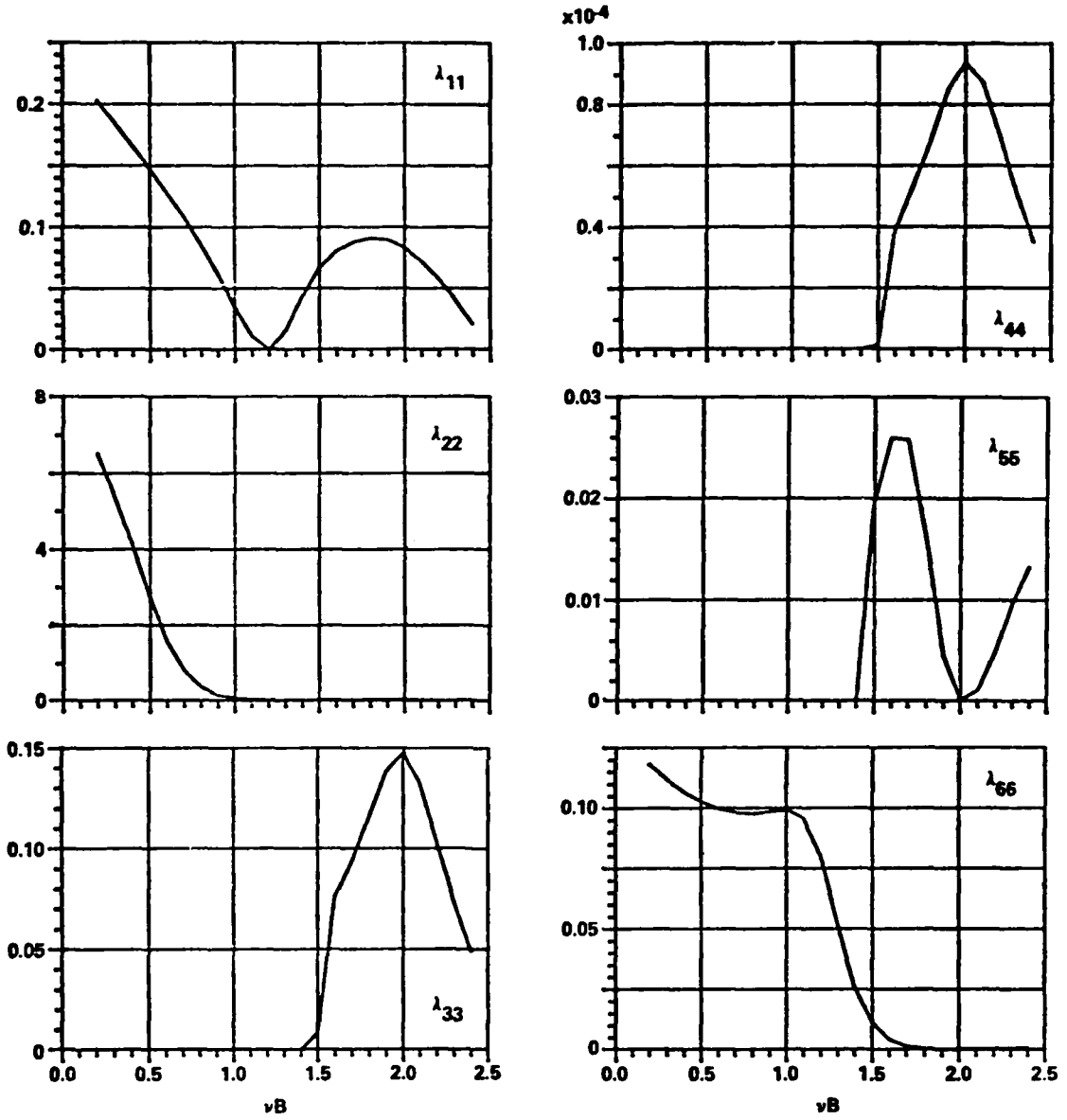


**Figure 4 — Damping Coefficients, $\lambda_{ij}$ versus $\nu B$, for $s/B = 0$**

damping coefficients and that of wave excitations corresponding to each mode of motion in the range of the values $\nu B = 0.2$ through 1.44. This is not a coincidence because there exist, for $\nu B < 1.44$, only a purely two-dimensional radiating wave (see the text following Equation (21)). On the other hand, if the wavelength becomes short and if there exist many modes of the three-dimensional wave system, then this similarity may no longer hold.

In Figure 7, the hydrodynamic coefficients computed from a purely two-dimensional problem in the yz-plane ($x = 0$) are presented as mentioned earlier. These computations are made because the added mass and moment of inertia of added-mass coefficients are mainly dependent upon the local flow field. Therefore, a two-dimensional result may be expected to provide some qualitative check because the ship is long compared with the length scale of the mid-ship cross-section in our problem at hand. In nondimensionalizing our two-dimensional hydrodynamic coefficients, we assume that the two-dimensional problem has a unit length so that the nondimensionalization of the hydrodynamic coefficients will be consistent with the definition given in Equations (23).

As expected, comparisons of $\mu_{33}$ and $\mu_{44}$ in Figure 3 and $\mu_{34}$ in Figure 5, with $\mu_{33}$, $\mu_{44}$, and $\mu_{34}$ in Figure 7, show remarkable similarities between them, except that the locations of the spikes in two- and three-dimensions are somewhat different: the spikes in the values of $\mu_{33}$, $\mu_{44}$, and $\mu_{34}$ occur at $\nu B = 0.784$ in two-dimensions and at $\nu B$

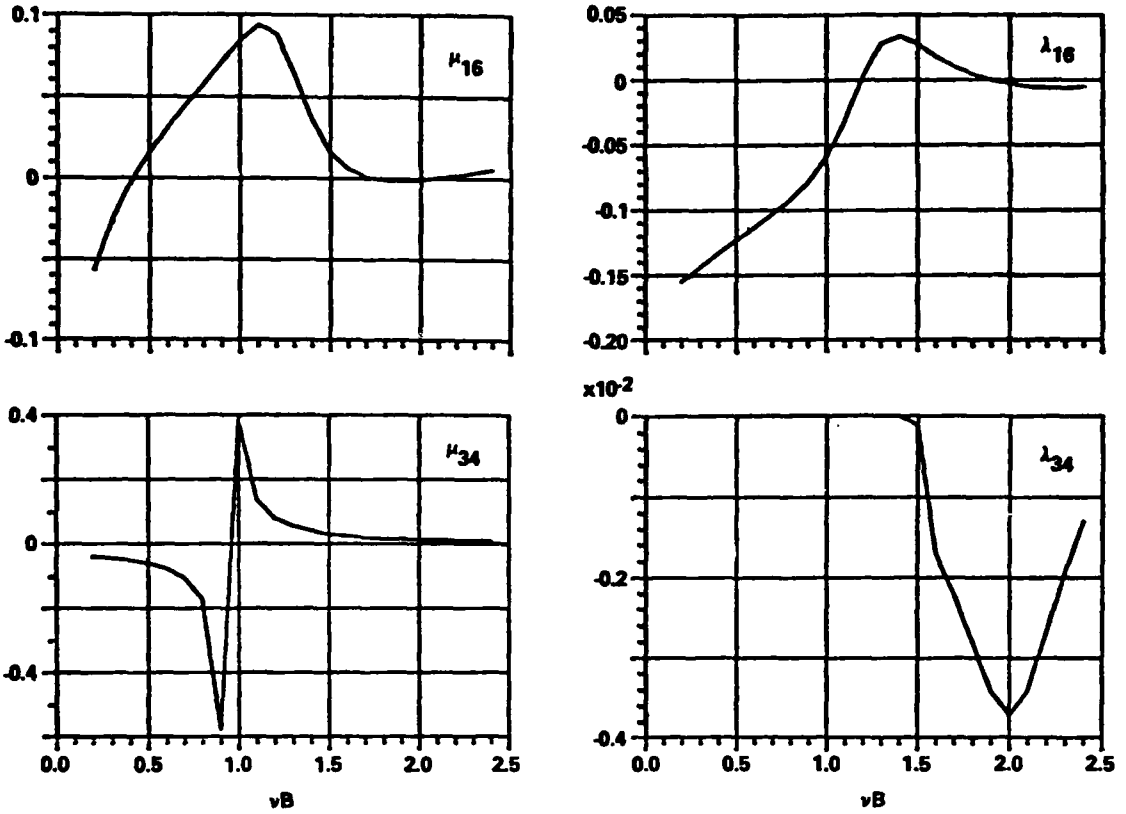


**Figure 5 — Coupling Hydrodynamic Coefficients, $\mu_{ij}$ and $\lambda_{ij}$ versus νB, for s/B = 0**

= 0.9 through 1.0 in three-dimensions. Comparison of the heave added-mass coefficient $\mu_{22}$ in Figure 3 with that in Figure 7 also shows a similarity in their qualitative behavior when $\nu B > 0.5$. However, when $\nu B < 0.5$, the three-dimensionality effect seems to be more significant, because the value of $\mu_{22}$ increases in three-dimensions, while it decreases more rapidly in two-dimensions, as νB decreases from 0.5 to 0.2.

A close examination of the local flow field at the midship cross-section corresponding to both positive and negative peaks, for example, in the sway added mass coefficient $\mu_{33}$ in Figures 3 and 7, shows that the relative fluid motion under the ship is out of phase for the positive and in phase for the negative values of added mass. In order to have a close examination on the location of these spikes, in addition, we also treated an eigenvalue problem corresponding to the foregoing two-dimensional boundary-value problem by a finite element method. When the finite element method is applied to the eigenvalue problem, the (original) eigenvalue problem defined in a partial differential equation reduces to a general matrix eigenvalue problem of a type $[A]\,\bar{X} = \lambda[C]\,\bar{X}$, where [A] and [C] are matrices and $\bar{X}$ is an eigenvector. In the present computations two sets of eigenvalue problems are solved. In the first set, [A] and [C] are identical to the matrices used in solving the boundary-value problem to obtain the results given in Figure 7. To obtain this set of matrices, 96 quadrilateral elements with a total of 345 nodes in the fluid and 18 nodes on the free surface are used. As a result, 18 eigenvalues and eigenvectors are obtained in the first set. In the second set, the submatrices are taken for [A] and [C] from the matrices constructed for our three-dimensional boundary-value problem at hand by retaining the matrix elements corresponding to the nodes at the midship cross-sectional plane. In the second set, in which a coarse mesh subdivision (total of 25 nodes) is used, four eigenvalues and eigenvectors are obtained.

The lowest nonzero eigenvalue is $\nu B = 0.78410$ in the first set which has fine mesh subdivisions and $\nu B = 0.82912$ in the second coarse mesh subdivisions. The higher modes of eigenvalues we computed are out of the range considered here. However, the location of the spikes occurring in our three-dimensional results, for example $\mu_{33}$ in Figure 3, is between $\nu B = 0.9$ and 1.0 not at $\nu B = 0.82912$. If we had solved a three-dimensional eigenvalue problem corresponding to the three-dimensional boundary-value problem treated in the present paper, we could have obtained eigenvalues all of which have a nonzero imaginary part. However, the three-dimensional eigenvalue problem is not treated here. The eigenvalues of the two-dimensional problem treated here are all real. From the comparisons among the two lowest eigenvalues, $\nu B = 0.78410$ and 0.82912, and the location of the spikes in the present three-dimensional numerical results ($\mu_{33}$, $\mu_{44}$, and $\mu_{34}$, i.e., νB is between 0.9 and 1.0), we can conclude that the difference in the locations of the spikes in $\mu_{33}$ in Figures 3 and 7 is caused partially by the inaccuracy in our three-dimensional computations (due to the use of not-fine-enough mesh subdivisions) and partially by the nature of three-dimensionality.

It should be kept in mind that in the values of $\mu_{22}$ in Figure 7, if we had computed $\mu_{22}$ at $\nu B = 0.7841$, then we could have noticed a singular behavior like the spikes

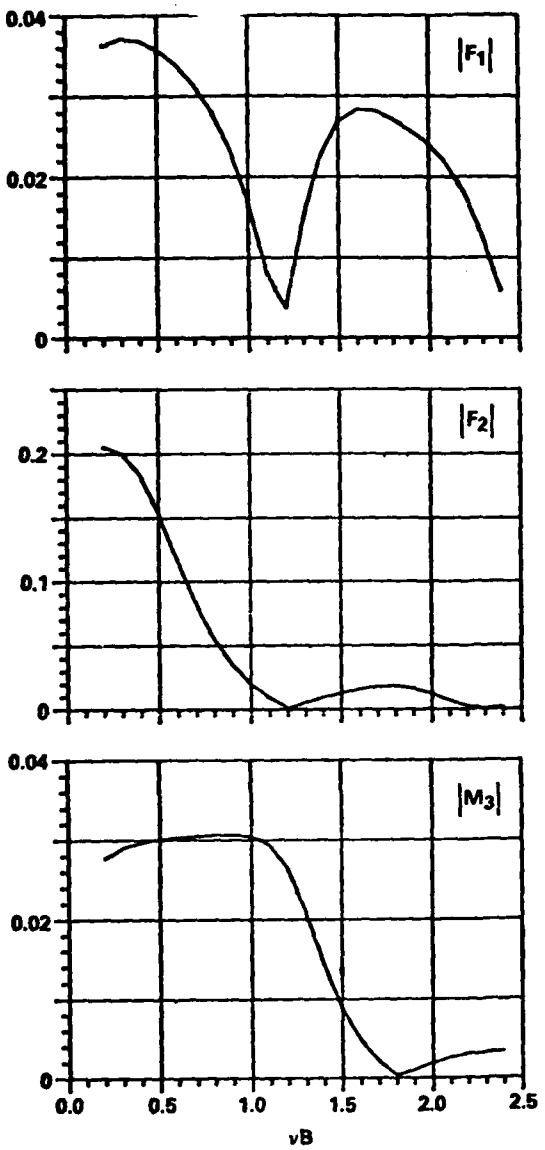


**Figure 6 – Magnitudes of Excitation Forces and Moment versus νB**

shown in the other curves, i.e., the resulting matrix equation for the eigenvalues being singular. It seems that the singular behavior of $\mu_{22}$ is much more localized than the other coefficients in Figure 7.

It is of interest to note that one can predict the lowest nonzero eigenvalue in the foregoing problem by a simple one-dimensional analysis as if treating a U-shaped pipe filled with water. This simple analysis gives the lowest eigenvalue, $\nu B = 2/3$, for the present case, which is not too bad. One can improve this value by introducing a few elementary potential functions, i.e., x, y, and $x^2 - y^2$, in a few finite elements, and performing simple integrations, as was done in Bai[6]. This improved approach gives the lowest eigenvalue, $\nu B = 0.75$. A more detailed finite element method applied to hydrodynamic eigenvalue problems will be reported in a separate paper in the near future.

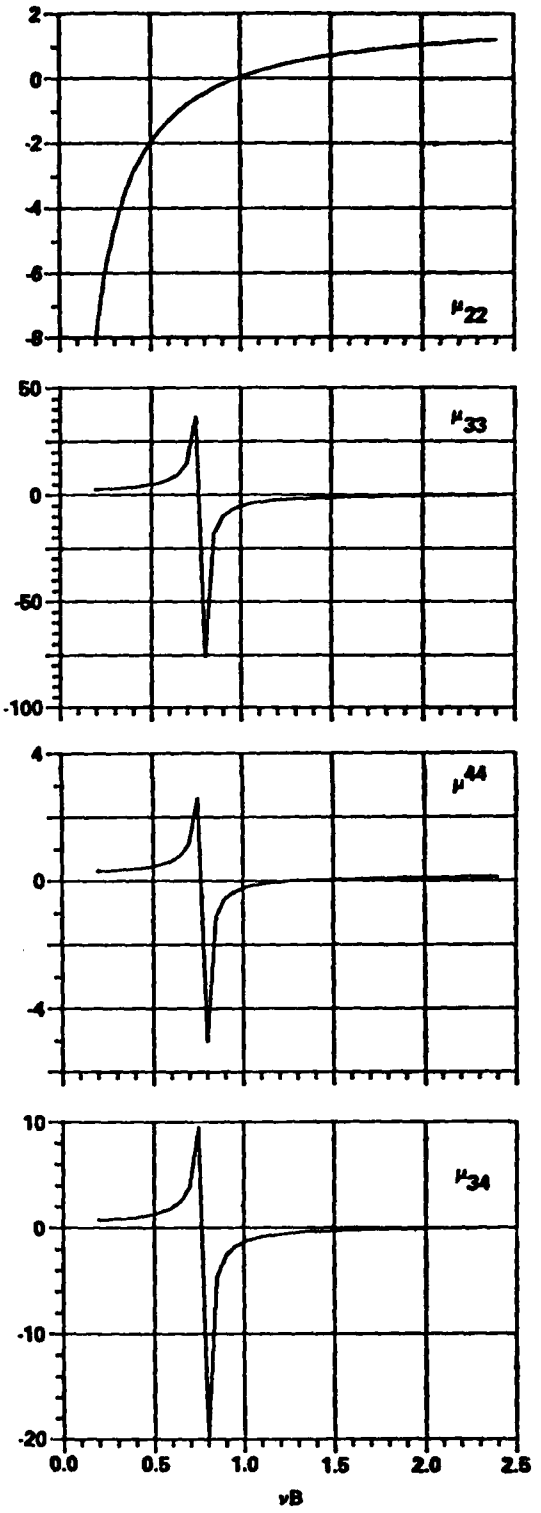


**Figure 7 – Purely Two-Dimensional Added Masses and Moment of Added Mass versus νB (Due to the side walls, no wave radiation is present.)**

We anticipated some singular behavior near $\nu B$ = 1.44, which is the first mode of the canal resonance. So we made additional computations around this value (excluding this value as discussed earlier) by taking finer intervals in $\nu B$. Our computed results do not show any abnormality like spikes, contrary to our anticipation.

In Figures 8 through 10, the hydrodynamic coefficients, $\mu_{ij}$ and $\lambda_{ij}$, are shown for the case of an off-center location of a ship in a canal, s/B = 0.125. The excitation forces and moments for this case are shown in Figure 11. The general behavior of all results for an off-center case is similar to those previously shown, except that the appearance of more sudden spikes is observed. The values of $\mu_{11}$, $\mu_{55}$, and $\mu_{66}$ in Figure 8 show spikes at $\nu B$ = 1.2 and 1.3. The values of $\mu_{22}$, $\mu_{33}$, and $\mu_{44}$ have spikes at $\nu B$ = 0.9 and 1.0 in the same figure. Of interest is that the values of $\mu_{11}$, $\mu_{22}$, and $\mu_{66}$ in Figure 8 and $\mu_{16}$, $\lambda_{16}$, and $\lambda_{34}$ in Figure 10 show spikes which were not shown in the previous case (s/B = 0). This can be interpreted in the sense that the range of the influence of the local eigenvalues is larger in the case of s/B = 0.125 than in the case of s/B = 0.

Similar spikes are also observed in the damping coefficients in Figure 9. The damping coefficients $\lambda_{33}$ and $\lambda_{44}$ reach a maximum peak at $\nu B$ = 1.0 and for $\lambda_{55}$ at $\nu B$ = 1.2. Some of the coupling hydrodynamic coefficients are shown in Figure 10. The magnitudes of wave excitation forces and moments are shown in Figure 11. The behavior of wave excitation forces and moments are very similar to the damping coefficients corresponding to motion which has already been discussed in the previous case of s/B = 0.

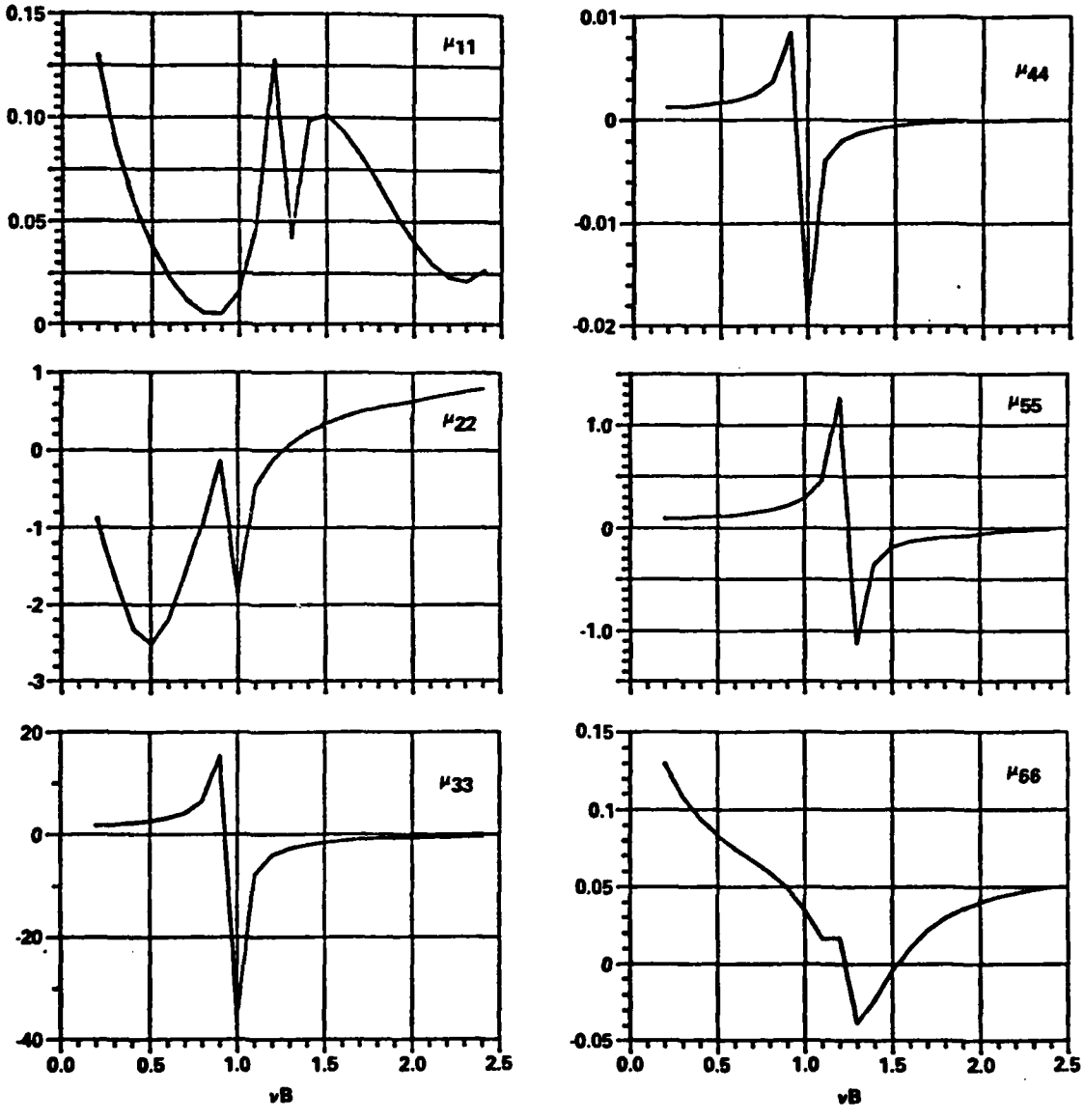


**Figure 8 — Added Masses and Moments of Inertia of Added Mass, $\mu_{ij}$ versus $\nu B$, for s/B = 0.125 (Off-Center)**

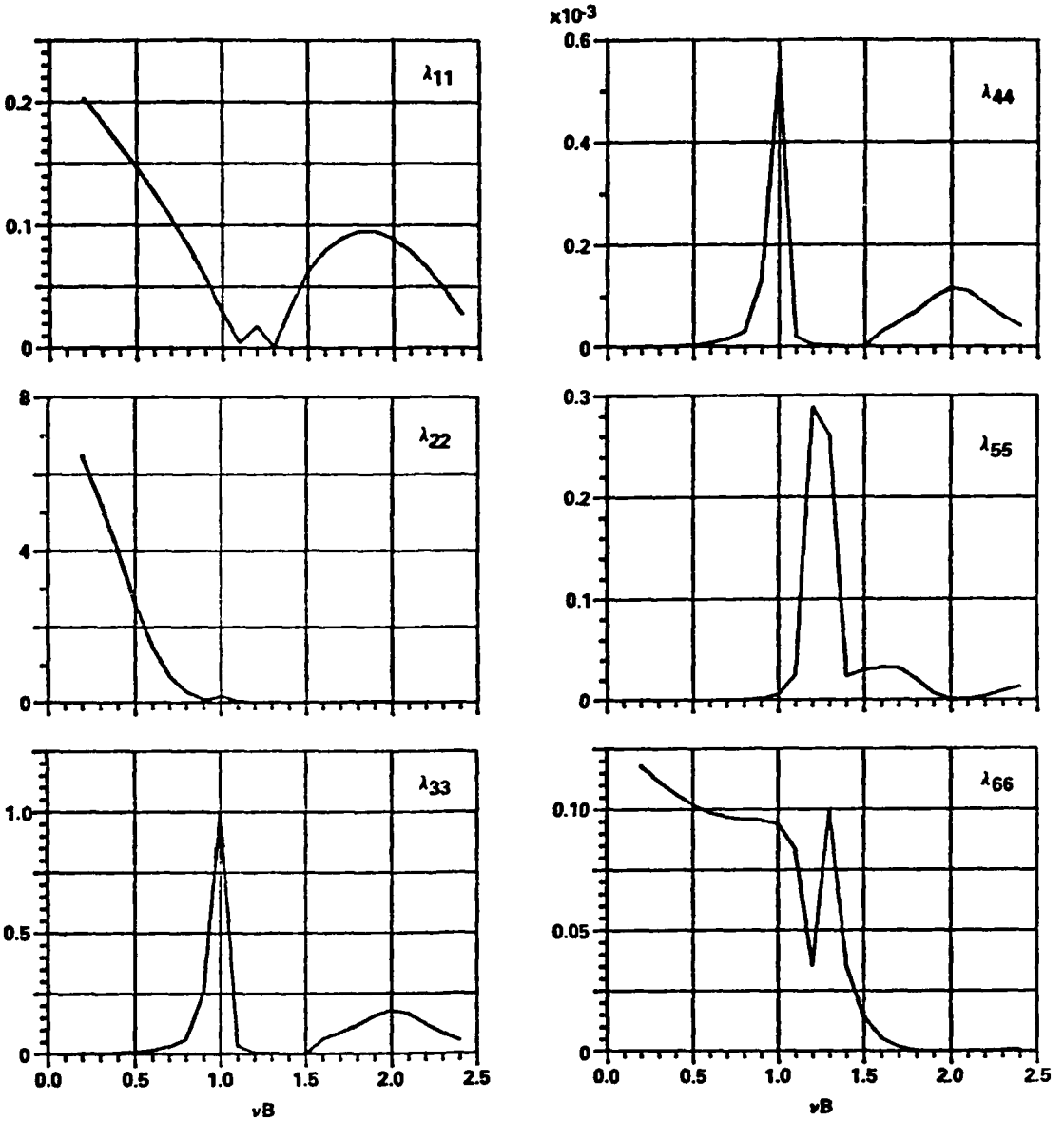


**Figure 9 — Damping Coefficients, $\lambda_{ij}$ versus $\nu B$, for $s/B = 0.125$**

In Figure 12, the six hydrodynamic coefficients were computed by treating a purely two-dimensional restricted water problem (ship located at off-center) with no radiating wave present, as discussed earlier in connection with Figure 7. We computed two sets of eigenvalues as in the previous case: the smallest (nonzero) eigenvalue for this case is $\nu B = 0.81140$ computed with the fine mesh subdivisions, and is $\nu B = 0.85796$ computed with coarse mesh subdivisions which give submatrix corresponding nodes at the midship-section plane at $x = 0$ taken from the three-dimensional problem. When we compare these eigenvalues with those obtained earlier for $s/B = 0$, the smallest eigenvalue increases when a ship at the canal's center moves away from the center.

Most of the discussions given in the previous case of $s/B = 0$ hold for the present case of $s/B = 0.125$. From the results and discussions presented here, it seems necessary to make more refinements in future investigations. In the present investigation, we concentrated mainly on the application of the localized finite element method to solve a three-dimensional ship-motion problem by taking a simple geometry with coarse mesh subdivisions. However, we tested two slightly different methods of solving the matrix equation. In the first method the final matrix which is complex banded and symmetric is solved by a Gaussian elimination. In the second method, we solve the real, banded symmetric submatrix equation first and then solve a rather small complex full-matrix equation. In the second

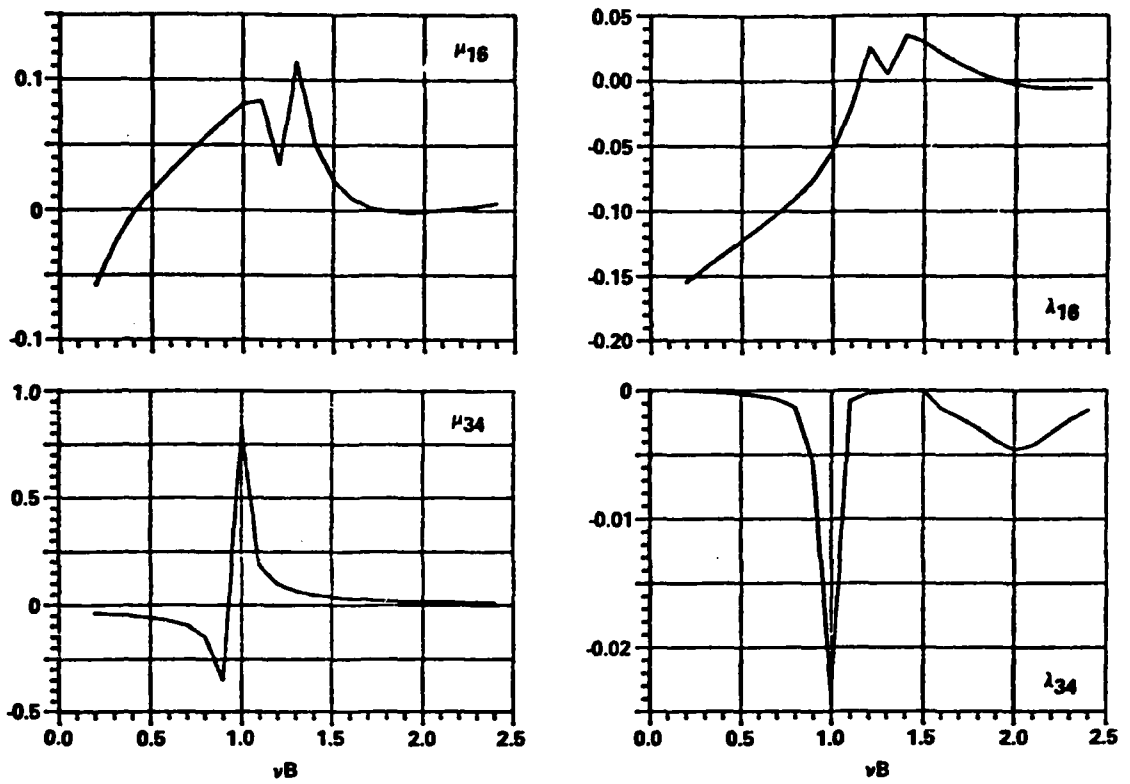


**Figure 10 — Some of Coupling Hydrodynamic Coefficients versus νB for s/B = 0.125**

method, the main core memory space can be reduced by half roughly. The Central Processor Unit Time in the CDC 6600 was approximately 40 seconds to compute six motions and one diffraction problem for one wave number by solving the complex matrix directly. By the second method, approximately 20 percent of the total CPU time was saved. In the present computer program, a considerable amount of time is used for the input-output operation due to out-of-core storage use.


### Acknowledgements

The author is grateful to Mr. Fredd Thrasher for his help in obtaining computer plots in this paper. The author is also grateful to Professor Daniel Euvrard, Drs. A. Jami, M. Lenoir, and D. Martin at ENSTA for many helpful discussions.


### References


1. Wehausen, J.V. and Laitone, E.V., 1960, "Surface Waves," Handbuch der Physik, Vol. IX, Springer-Verlag, Berlin, pp. 446-778.

2. Bai, K.J., and Yeung, R.W., 1974, "Numerical Solutions to Free Surface Flow Problems," The Tenth Symposium on Naval Hydrodynamics, Office of Naval Research, held at MIT, Cambridge.

3. Bai, K.J., 1972, "A Variational Method in Potential Flows with a Free Surface," Ph.D. dissertation, Dept. of Naval Architecture, Univ. of California, Berkeley.

4. Bai, K.J., 1975, "Diffraction of Oblique Waves by an Infinite Cylinder," J. Fluid Mechanics, Vol. 68, pp. 513-535.

5. Bai, K.J., 1976, "The Added Mass and Damping Coefficients of and the Excitation Forces on Four Axisymmetric Ocean Platforms," David W. Taylor Naval Ship R&D Center, Bethesda, SPD-670-01.

6. Bai, K.J., 1977, "The Added Mass of a Rectangular Cylinder in a Rectangular Canal," J. Hydronautics, Vol. 11, pp. 29-32.

7. Berkhoff, J.C.W., 1972, "Computation of Combined Reffraction - Diffraction," Proc. 13th Coastal Engineering Conference, Vol. 2, pp. 471-490.

8. Smith, D.A., 1974, "Finite Element Analysis of the Forced Oscillation of Ship Hull Forms," M.S. Thesis, Naval Postgraduate School, Monterey.

9. Chen, H.S. and Mei, C.C., 1974, "Oscillations and Wave Forces in a Man-Made Harbor in the Open Sea," The Tenth Symposium on Naval Hydrodynamics, Office of Naval Research, held at MIT, Cambridge.

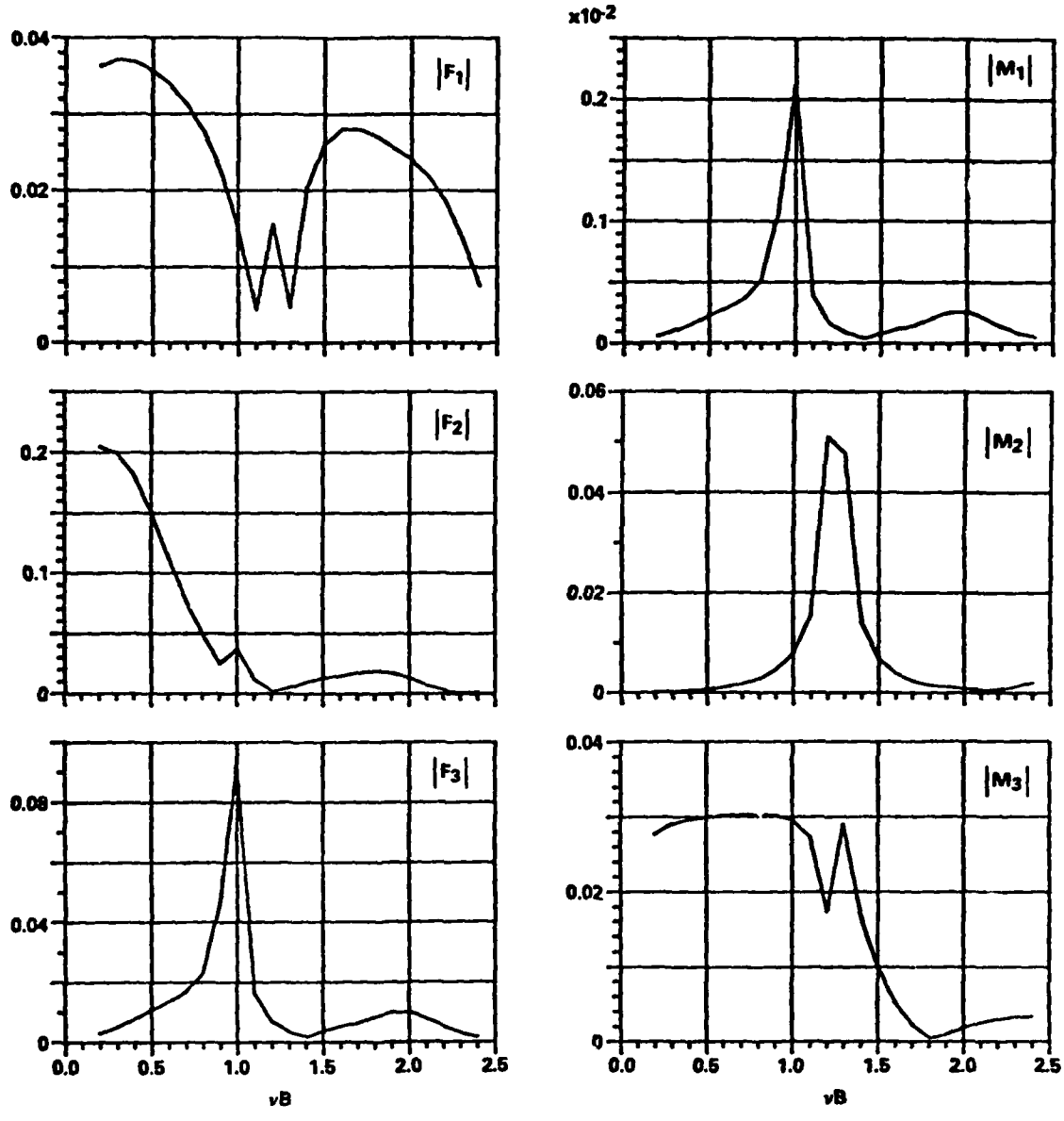


Figure 11 – Magnitudes of Wave Excitation Forces and Moments versus $\nu B$


10. Seto, H. and Yamamoto, Y., 1975, "Finite Element Analysis of Surface Wave Problems by a Method of Superposition," The First International Conference on Numerical Ship Hydrodynamics, DTNSRDC, Bethesda, pp. 49-70.

11. Yue, D.K.P., Chen, H.S., and Mei, C.C., 1976, "Three-Dimensional Calculations of Wave Forces by a Hybrid Element Method," The Eleventh Symposium on Naval Hydrodynamics, Office of Naval Research, pp. 325-332.

12. Euvrard, D., Jami, A., Morice, C., and Ousset, Y., 1977, "Calcul Numerique des Oscilations d'un Navire Engendrees par la Houle," Part I & II, J. Mecanique, Vol. 16, No. 2, pp. 289-326, No. 3, pp. 327-394.

13. Chowdbury, P.C., 1972, "Fluid Finite Elements for Added-Mass Calculations," Int. Shipbuilding Progress, Vol. 19, No. 217, pp. 302-309.

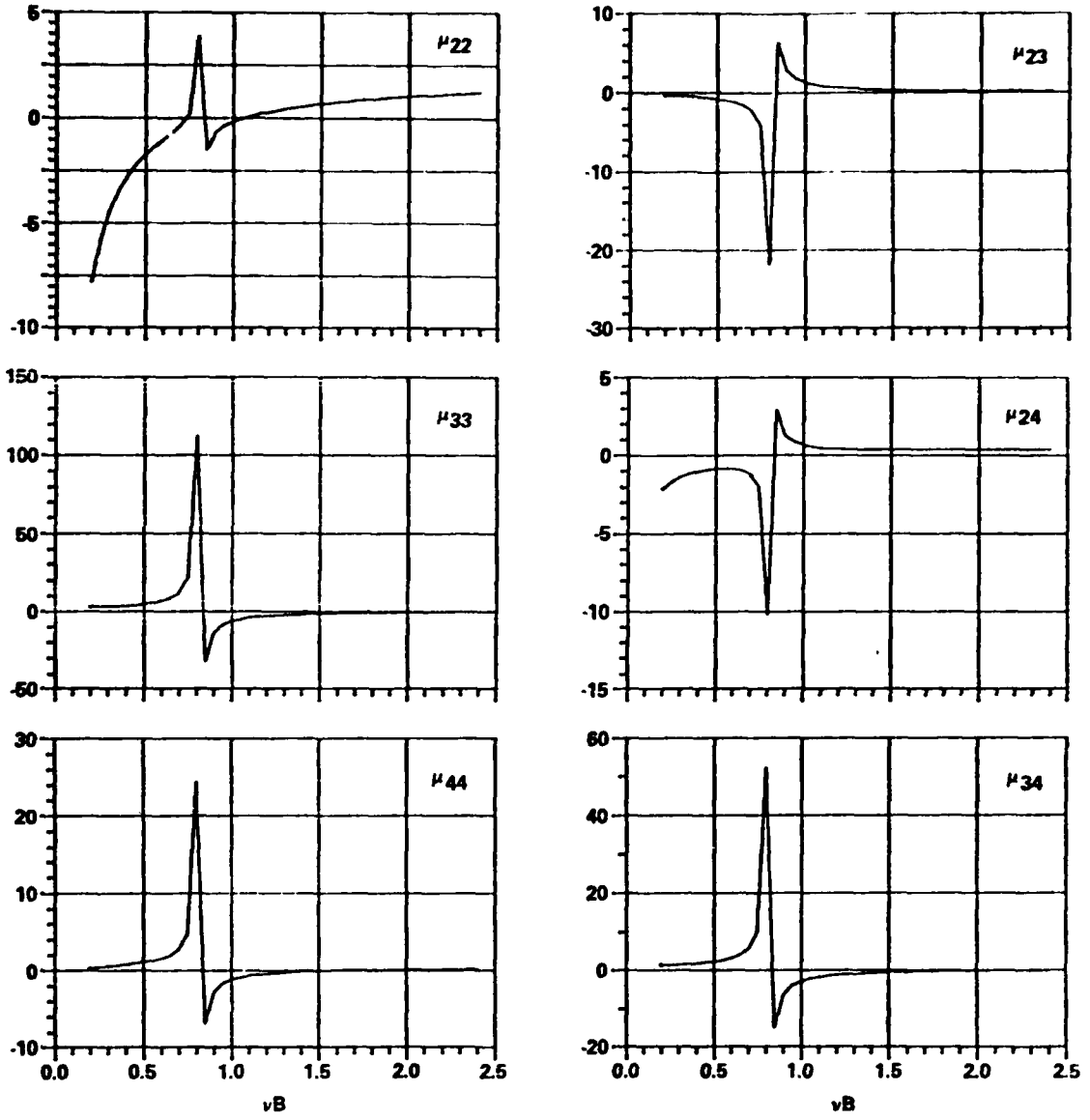


**Figure 12 — Purely Two-Dimensional Added Masses and Moment of Added Mass versus νB for s/B = 0.125 (Due to the side walls, no wave radiation is present.)**

## INITIAL DISTRIBUTION

| Copies | |
|---|---|
| 1 | CHONR/Lib |
| 1 | NRL/Lib |
| 5 | NAVSEA<br>1 03R2<br>1 32131<br>1 32132<br>1 32133<br>1 31211 (Kennel) |
| 2 | USNA<br>1 Lib<br>1 Bhattacharyya |
| 1 | NAVPGSCOL Lib |
| 1 | NROTC & NAVADMINU, MIT |
| 1 | NADC |
| 1 | NOSC/Lib |
| 12 | DTIC |
| 2 | HQS COGARD |
| 1 | MARAD |
| 2 | MMA<br>1 Lib<br>1 Dr. McClean |
| 1 | NSF ENGR DIV LIB |
| 2 | U CAL BERKELEY/DEPT NOAF<br>1 NOAF Lib<br>1 Wehausen |
| 1 | FLORIDA ATLANTIC U OE LIB |
| 2 | U HAWAII/Bretschneider |

| Copies | |
|---|---|
| 3 | MIT<br>1 Barker Eng Lib<br>1 Ocean Engr/Sclavounos<br>1 Ocean Engr/Yeung |
| 1 | ORI, INC/Kim |
| 1 | ST JOHNS U/Hsieung |
| 1 | SWRI/Applied Mech Review |
| 1 | BOEING ADV AMR SYS DIV |
| 1 | SIT DAVIDSON LAB/Lib |
| 2 | WEBB INST<br>1 Ward<br>1 Hadler |
| 1 | SNAME |
| 1 | HYDRONAUTICS |
| 1 | SCIENCE APPLICATIONS, INC./ ANNAPOLIS/Salvesen |
| 1 | UNIV WASHINGTON/Mech Engr/Adee |
| 1 | MARITIME RES INF SERVICE |
| 2 | U MICHIGAN ANN ARBOR/DEPT NAME<br>1 Beck<br>1 Troesch |

### CENTER DISTRIBUTION

| Copies | Code | Name |
|---|---|---|
| 1 | 1113 | Lamb |
| 1 | 1115 | Allen |
| 1 | 1504 | Monacella |
| 1 | 156 | Cieslowski |
| 1 | 1506 | Fein |

| Copies | Code | Name |
|---|---|---|
| 1 | 152 | Lin |
| 1 | 1521 | Day |
| 1 | 1522 | Wilson |
| 1 | 1522 | Kim |
| 1 | 1523 | Koh |
| 1 | 154 | McCarthy |
| 1 | 154 | Yim |
| 1 | 1542 | Huang |
| 30 | 1542 | Bai |
| 1 | 1542 | Chang |
| 1 | 1561 | McCreight |
| 1 | 1561 | O'Dea |
| 1 | 1562 | Hong |
| 1 | 1562 | Moran |
| 1 | 1563 | Russ |
| 1 | 1843 | Haussling |
| 10 | 5211.1 | Reports Distribution |
| 2 | 522.1 | Unclassified Lib (C) (m) |
| 1 | 522.2 | Unclassified Lib (A) |